WAVELET ANALYSIS OF BENDER ELEMENT SIGNALS

Julien Bonal, Shane Donohue, Ciaran McNally

School of Architecture, Landscape and Civil Engineering, University College Dublin, Ireland.

Corresponding author: Dr. Shane Donohue, School of Architecture, Landscape and Civil Engineering, University College Dublin (UCD), Newstead, Belfield, Dublin 4, IRELAND.
Tel: +353-87-9711917; Fax: +353-1-7163297
e-mail: shane.donohue@ucd.ie

Keywords: Wavelet, Bender element, signal processing, singularity

ABSTRACT

Accurate determination of shear wave arrival time using bender elements may be severely affected by a combination of near field effects and reflected waves. These may mask the first arrival of the shear wave, making its detection difficult in the time domain. This paper describes an approach for measuring the shear wave arrival time through analysis of the output signal in the time-scale domain using a multi-scale wavelet transform. The local maxima lines of the wavelet transform modulus are observed at different scales and all singularities are mathematically characterised, allowing subsequent detection of the singularity relating to the first arrival. Examples of the use of the approach on typical synthetic and experimental bender element signals are also supplied, and these results are compared to those from other time and frequency domain approaches. The wavelet approach is not affected by near field effects and instead is characterised by a relatively consistent singularity related to the shear wave arrival time, across a range of frequencies and noise levels.

INTRODUCTION

The measurement of shear stiffness at small strain (G_{max}) is useful for predicting deformation of soil, as strains associated with most soil-structure interaction problems are generally less than 0.1% (Jardine et al. 1986). It has been shown by Stokoe et al. (2004) that stiffness-strain curves for a range of materials may result in poor estimates of deformation if small strain stiffness values have not been considered. There are several techniques available for measuring this parameter, both in-situ and in the laboratory, a number of which involve measurements of the velocity of a seismic shear wave, and corresponding calculation of G_{max} from:

$$G_{\max} = \rho V_s^2 \quad (1)$$

where V_s is the shear wave velocity and ρ is the density of the soil. One such popular approach, initially developed by Shirley & Hampton (1978) and later by Dyvik & Madshus (1985), involves using bender elements, piezoelectric transducers capable of generating and detecting shear or compressional (Lings & Greening. 2001) motion. Bender elements are relatively cheap, can be wired quite simply (Santamarina et al. 2001) and they may easily be incorporated into a range of laboratory geotechnical testing apparatus (Dyvik & Olsen 1989; Viggiani & Atkinson 1995a; Jovicic & Coop 1997; Zeng & Ni 1998), in addition to being useful in the field on soil samples extracted from the ground (Donohue & Long 2010). Bender elements are now more popular than ever and their use has now extended beyond the academic field, and into industry. Despite this popularity there is, however, no definitive methodology for using bender elements, and interpretive procedure may vary considerably from one user to the next.

In order to determine V_s using bender elements only two measurements are required, the travel distance between source and receiver, and the travel time. Travel distance is

relatively easy to determine and involves measuring the distance between transmitter and receiver tips (Viggiani & Atkinson 1995b). Measurement of the travel time is, however, much more problematic as the received signal is usually significantly altered from the input transmitted signal. By far the most commonly used approach is to estimate the first arrival of the shear wave from a visual inspection of the received signal (Fig. 1). However, due to near field effects and wave reflections from sample boundaries, this approach may result in significant error in travel time interpretation. The significance of near field effects in bender element testing has been discussed by at length by Brignoli et al. (1996), Viggiani & Atkinson (1995b), Jovicic et al. (1996), Arroyo et al. (2003) and Lee & Santamarina 2005. Sanchez-Salinero et al. (1986), with a multiple aligned receiver, field cross hole geophysical survey in mind, produced numerical evidence that near field effects may mask the shear wave first arrival and proposed the following limit for interpretation of bender element signals:

$$2 < \frac{d}{\lambda} < 4 \qquad (2)$$

where d is the distance between elements and λ is the wavelength. The lower limit was proposed to take into account near field effects, whereas the upper limit was proposed to minimize signal attenuation. Taking into account these recommendations, Kawaguchi et al. (2001) suggested selecting point 3 in Fig. 1 as the correct first arrival. Even with strong receiver signals, however, Donohue (2005) showed that each of these points may remain frequency dependent significantly above the upper limit of Sanchez-Salinero et al. (1986). After consideration of Stokes's fundamental solution for an isolated source, Arroyo et al. (2003) suggested that measurements in the far field may not be sufficient to ensure adequate measurement precision.

A number of authors have suggested alternative approaches for travel time interpretation, based in both the time and frequency domains (e.g. Viggiani & Atkinson

1995b; Brocanelli & Rinaldi 1998; Blewett et al. 1999; Mohsin et al 2004). Arulnathan et al. (1998) suggested using multiple reflections to overcome both travel distance and travel time uncertainties, with Lee & Santamarina (2005) recommending cross correlation of the first and second arrival events to provide accurate travel times. Multiple reflections are, however, not always apparent, and their presence may be dependent on the degree of attenuation that occurs as the wave travels through the soil sample. Cross correlation was also suggested by Viggiani & Atkinson (1995b), Mohsin et al. (2004) and Wang et al. (2007). Mohsin et al. (2004) developed an automated system for measuring travel time based on cross correlation. This approach required measurements of all cross correlation peaks over a range of confining stresses. Wang et al. (2007) recommended the cross correlation approach only if the near-field effect is not pronounced and the two receivers possess very similar transfer functions.

Another frequency domain approach to have gained popularity over recent years is the phase-delay method, which was first used by Viggiani & Atkinson (1995b) for bender element testing and discussed more recently by Arroyo et al. (2003) and Greening & Nash (2004). Using this technique, Arroyo et al. (2003) developed a criterion for ensuring that velocity measurements are made outside the influence of the near field. Greening et al. (2003), however, reported that this approach consistently produces lower estimates of V_s when compared to time domain measurements. Brandenberg at al. (2008), made use of wavelets, although in a different manner to that demonstrated in this paper, to measure shear wave travel times. They observed that travel times measured by wavelet correlation are less sensitive to noise and near field effects than manual travel time picks. Arroyo (2007) also tested wavelets on bender element signals and developed a means of interpreting the output signal using transform ridges.

This paper will discuss the use of a wavelet based approach for arrival time determination. The background theory is outlined and examples, both numerical and

experimental, are provided illustrating the use and practical application of the approach for bender element testing.

WAVELETS FOR SIGNAL ANALYSIS

A signal may be observed through two main domains: time domain and frequency domain, as illustrated in Fig. 2. The Fourier Transform and its inverse connect these domains and are the main mathematical tools for signal analysis. The Fourier Transform is perfectly adequate for stationary and periodic (or quasi-periodic) signals and provides a global description of frequency distribution, energy and overall regularity. However, it involves the complete loss of local time information such as the location of singularities (corresponding to local variations in the smoothness of the signal). Keeping local time information makes non-stationary signal analysis possible. The Windowed (or Short Time) Fourier Transform is a time-frequency tool. However the resolution of this tool is limited by Heisenberg's principle: as the accuracy in the time domain increases, the accuracy in the frequency domain decreases.

A wavelet is a mathematical function used to divide a given function or continuous time signal into different frequency components and study each component with a resolution that matches its scale. A wavelet transform is the representation of a function by wavelets. The wavelets are scaled and translated copies (known as "daughter wavelets") of a finite length or fast-decaying oscillating waveform (known as the "mother wavelet"). Wavelet transforms have advantages over traditional Fourier transforms for representing functions that have discontinuities and sharp peaks, and for accurately deconstructing and reconstructing finite, non-periodic and/or non-stationary signals.

The Wavelet Transform is motivated by the possibility of finding a singularity, it decomposes a signal into elementary building blocks that are well localized both in time and

frequency (Mallat & Hwang, 1992). The local detail is matched to the scale of the wavelet, so it can characterize coarse (low frequency) features on large scales and fine (high frequency) features in small scales. This mathematical tool is a time-scale and multi-resolution analysis that allows the user to overcome the uncertainty issues described by Heisenberg's principle by applying the wavelet at several scales.

Continuous Wavelet Transform (CWT)

The CWT is a mathematical tool which was first introduced by Grossmann & Morlet (1984). To define the CWT, consider $\Psi(t)$ be a complex valued function. The function is said to be a wavelet if and only if its Fourier transform $\hat{\psi}(\omega)$ satisfies:

$$\int_0^{+\infty} \frac{|\hat{\psi}|^2}{\omega} d\omega \quad = \quad \int_{-\infty}^{0} \frac{|\hat{\psi}|^2}{\omega} d\omega \quad = \quad C_\psi \quad with \quad C_\psi < +\infty \tag{3}$$

This condition for zero mean implies that:

$$\int_{-\infty}^{+\infty} \psi(t) dt \quad = \quad 0 \tag{4}$$

Let Ψ be the mother wavelet that generates a large family by dilation. Therefore $\psi_S(t) = 1/s \times \psi(t/s)$ is the dilation of $\Psi(t)$ by the factor scale s. This factor changes the local frequency by dilation or compression of the wavelet. The CWT of a function f, in Hilbert space $L^2(\mathbf{R})$, is the convolution of f and Ψ_S as defined by :

$$Wf(s,t) \quad = \quad f * \psi_S(t) \quad = \quad \int_{-\infty}^{+\infty} f(u).\overline{\psi_S(t-u)} du \tag{5}$$

This definition can be written using the main wavelet:

$$Wf(s,t) \quad = \quad f * \frac{1}{s}\psi(\frac{t}{s}) \quad = \quad \frac{1}{s}\int_{-\infty}^{+\infty} f(u).\overline{\psi(\frac{t-u}{s})} du \tag{6}$$

In practical applications, the computation of CWT may consume a significant amount of time and resources. Also, waveforms are recorded as discrete time signals and can be analysed by numerical algorithms using the Discrete Wavelet Transform (DWT), as an approach proposed by Mallat (1999). The signal S can be represented as a series of signals {$Wf(2^1,t)$, $Wf(2^2,t)$,..., $Wf(2^N,t)$, d^N} where N is the maximum scale factor. {$Wf(2^1,t)$, $Wf(2^2,t)$,..., $Wf(2^N,t)$} characterise the fine structure of the main signal along power of two scales {2^1, 2^2,…, 2^J}. Daubechies (1992) showed that the original signal can be reconstructed completely and analysed at different resolutions using the inverse DWT.

SINGULARITY DETECTION IN OUTPUT SIGNAL

The fundamental reason for applying wavelets to bender element tests is to allow detection of the point of first arrival of the shear wave, represented by a singularity in the signal. This may be, however, disguised by the presence of a near field effect due to the compressive wave and noise. To resolve these complications, the approach of Mallat & Hwang (1992) is utilised, whereby they characterised the local smoothness of a signal by its local Lipschitz exponent.

In practical terms, the shear wave generated for bender element testing follows a sine wave and may be defined by:

$$S(t) = \begin{cases} S_0 \sin\left(\dfrac{2\pi(t-t_s)}{T_i}\right) & if\ t_s < t < t_s + T_i \\ 0\ otherwise \end{cases} \qquad (7)$$

Although S is a continuous function, it does have two singular points at t_s (first arrival time) and (t_s+T_i) as its first derivative is discontinuous at t_s and (t_s+T_i). The theory presented by Arroyo et al. (2003) offers the possibility to directly calculate the displacement at the receiver probe induced by the wave from the input probe. The direct shear wave is the perpendicular

movement of Stokes' fundamental solution describing the movements generated by a unit impulsive force isolated in an infinite elastic medium.

$$\begin{aligned} &\vec{u}_s = \vec{u} \wedge \vec{r} = (\vec{b} \wedge \vec{r}) * [F_S - N] \\ &where \quad F_S = \frac{k}{v_S^2}\, \delta(t - \frac{r}{v_S}) \\ &\qquad N = \frac{kt}{r^2} [H(t - \frac{r}{v_P}) - H(t - \frac{r}{v_S})] \end{aligned} \tag{8}$$

where $\vec{r}$ is the direction of propagation, $\vec{b}$ is the forcing, $k = 1/4\pi\rho r$, r is the distance from the source, t is the time, v_S is the shear wave velocity, v_P is the compressive wave velocity, H is the Heaviside step function and δ is the Dirac function.

Using Equation 8, and after several operations, the displacement generated by a unit direct shear wave at the tip of the receiver probe $u(L_{tt},t)$ is composed of two parts : the far-field component u_F and the near-field component u_N. The expression of u_F is exactly the same as the input and translated into the time domain. However, the expression of u_N is more complicated.

$$u_F(L_{tt},t) = \frac{k}{v_S^2} \sin(\omega_i(t - t_S))\, [H(t - t_S) - H(t - t_S - t_i)] \tag{9}$$

$$\begin{aligned} u_N(L_{tt},t) = &-\frac{k\, t_i}{4 v_S^2 t_S^2 \pi} \{2\pi t [H(t_P - t) - H(t_S + t_i - t) - H(t_S - t) + H(t_P + t_i - t)] \\ &+ 2\pi t_i\, [H(t_P + t_i - t) - H(t_S + t_i - t)] \\ &+ [2\pi t_P \cos(\omega_i(t - t_P)) + t_i \sin(\omega_i(t - t_P))]\, [-H(t_P - t) + H(t_P + t_i - t)] \\ &+ [2\pi t_S \cos(\omega_i(t - t_S)) + t_i \sin(\omega_i(t - t_S))]\, [H(t_S - t) + H(t_S + t_i - t)] \end{aligned} \tag{10}$$

where t_p is the arrival time of the compressive wave and t_s is the arrival time of the share wave and ω_i is the input pulsation. Therefore, one can show by calculation that the near-field component u_N is a continuous function and its first derivative can always be prolonged by continuity everywhere.

Using the approach of Mallat & Hwang it is possible to measure the local regularity or smoothness of a function using the Lipschitz exponent, α. Consider a function $f(t)$ to be locally analogised to a polynomial of order n, $P_n(h)$, plus a non-integer exponent function, h^{α}, where $n \leq \alpha \leq n+1$. The function is said to be Lipschitz α at t_0 if and only if there exists two constants, A and $h_0 > 0$, and a polynomial of order n, $P_n(t)$, such that for $|h| < h_0$:

$$\left| f(t_0 + h) - P_n(h) \right| \leq A|h|^{\alpha} \qquad (11)$$

The function $f(t)$ is uniformly Lipschitz α over the interval]a,b[, if and only if there exists a constant A and for any $t_0 \in$]a,b[there exists a polynomial of order n, $P_n(h)$, such the Equation 11 above is satisfied if $(t_0+h) \in$]a,b[. Lipschitz regularity of $f(t)$ and t_0 is called the superior bound of all values α such that $f(t)$ is Lipschitz α at t_0. A function is said to be singular at t_0, if it is not Lipschitz 1 at t_0. The calculation of Lipschitz exponents is discussed in detail by Mallat & Hwang (1992). For this study it suffices to summarise the following points:

- As the scale goes to zero, all singularities of a function $f(t)$ can be located by following the maxima lines of its CWT, defined as any connected curve in the scale (s, t), along which all points are modulus maxima.
- It is possible to locally assess the Lipschitz exponent α when the scale s goes to zero. This allows the user to sort the singular points as a measure of local smoothness.
- The Lipschitz exponent of the idealised bender element signal (a sine wave) will take a value of 1 at the first arrival and will be infinite almost everywhere.
- The Lipschitz exponent of the theoretical near-field component will take a value of 2, allowing the user to differentiate from the 1st arrival singularities (Eq. 10).
- Noise in the signal can be considered to be Gaussian noise and will have a negative Lipschitz value, allowing the user to distinguish from other more relevant singularities which will have a positive Lipschitz exponent.

In practice, the regularity of a function at a point t_0 is characterised by the behaviour of its wavelet transform along any line that belongs to a cone strictly smaller than the cone of influence (Mallat & Hwang, 1992), where the width of this smaller cone is unknown. When analysing a signal, a huge number of maxima lines are obtained since the Gaussian noise creates singularities at any time. To distinguish noise from singularities of interest, the Lipschitz exponent is calculated using Mallat & Hwangs methodology.

Let *f(t)* be a tempered distribution whose wavelet transform is well defined over]a,b[and let t_0 be an element of]a,b[. We suppose that there exists a scale $s_0 > 0$, and a constant *C*, such that for $t \in$]a,b[and $s < s0$, all the modulus maxima of *Wf(s, t)* belong to a cone defined by:

$$\left|t - t_0\right| \leq Cs \tag{12}$$

Then, at all points $t_1 \in$]a,b[and $t_1 \neq t_0$, *f(t)* is uniformly Lipschitz *n* in a neighbourhood of t_1. Let $\alpha < n$ be a non-integer. The function *f(t)* is Lipschitz α at t_0, if and only if there exists a constant *A* such that at each modulus maxima *(s,t)* in the cone defined above

$$\left|\mathrm{Wf}(s,t)\right| \leq As^{\alpha} \tag{13}$$

This inequality is rewritten in a $\log_2$ to produce the following equation, which can be used to sort singularities into ranges of similar smoothness:

$$\log_2\left|\mathrm{Wf}(s,t)\right| \leq \log_2(A) + \alpha\log_2\left(2^j\right) = \log_2(A) + \alpha j \tag{14}$$

Wavelet Selection

Selection of a mother wavelet is driven by the need to match its features to our objectives. The mother wavelet is characterised by its support *K*, its number of vanishing moments and

its regularity; these considerations are discussed in detail by Mallat & Hwang (1992). Using these criteria a number of potential mother wavelets are compared in Table 1. For the purpose of this study the Symlet 7 wavelet was found to be the most suitable as it respects all of the key parameters.

ALGORITHM EMPLOYED

Using the principles outlined above, an algorithm was developed to identify singularities in bender element signals associated with the point of first arrival. The steps included are:

1) Extract relevant information from the data, such as sampling frequency *(f_r)* and input frequency *(f_i)*

2) Reshape the signal so that its length is the nearest 2^n just greater than the original signal length (this makes the wavelet decomposition more efficient).

3) Decompose the signal at the scales $\{2^1, 2^2, 2^3, \ldots\}$. This step will lead to the production of a DWT using the chosen wavelet at each scale. For example, consider the sample signal shown in Fig. 4. This signal is then decomposed using the Symlet 7 wavelet at different scales as shown in Fig. 5.

4) Maxima lines are detected across all discrete scales and each local Lipschitz exponents is estimated by linear regression on the scales from 2^1 to 2^6. Obviously, α is underestimated because the upper tangent line, given by Equation 14, has a higher slope than the regression line. All negative Lipschitz values (noise) are eliminated and singularities of interest retained.

5) The time information of the singularities of interest is retained and these are plotted on the original signal as shown in Fig. 6.

At this point the user must identify which of the potential singularities identified corresponds to the point of shear wave arrival. It is worth noting that the steps outlined above have all been programmed, but that the final interpretation must be conducted by the analyst.

TESTING THE WAVELET APPROACH

Synthetic Data Testing

In order to test the wavelet approach, a number of synthetic signals were generated using the approach Arroyo et al. (2003), who refined the numerical model of Sanchez-Salinero et al. (1986), using Stokes's fundamental solution for an isolated source. The wavelet technique was then applied to the synthetic signals of varying frequency, for which the true shear wave (1200 μs) and near field effect (1100 μs) arrival times were a known input. Gaussian noise was also applied to the synthetic signals at different levels (zero, 1%, 2%, 3% noise, where, for example 2% corresponds to a signal to noise ratio of 50). Synthetic signals and corresponding singularities with an input frequency of 2.5 kHz are shown in Figure 6 at different noise levels. All singularities detected between 800 μs and 1400 μs are shown. As mentioned above, the Lipschitz exponent of the theoretical near-field component will take a value of 2, thereby allowing the user to differentiate from the 1st arrival singularities. Taking this into account, all signals were examined for a lower range of Lipschitz exponents (0.5 - 1.6). As shown in Figure 6a, for a noise free synthetic signal, there is no singularity present at the travel time corresponding to the near field (1100 μs). By contrast, a consistent singularity, regardless of noise is always present at 1200 μs (± 5 μs), relating to the shear wave first arrival.

These synthetic tests were also used to determine the Lipschitz exponent corresponding to the true shear wave arrival for the different signal to noise ratios. Every singularity within 5 μs was identified and the corresponding Lipschitz exponent determined.

A summary of the results of these tests, and other tests at frequencies of 1 kHz and 7.5 kHz are provided in Table 2 and show that, as expected, the Lipschitz exponent corresponding to the true shear wave first arrival decreases with increasing noise level. Measured Lipschitz exponents, were however, higher than expected, particularly for those measured on signals containing zero noise. As discussed above, the Lipschitz exponent of the idealised bender element signal (a sine wave) should take a value of 1 at each wave arrival as the first arrival and will be infinite almost everywhere. The DWT, however, limits the accuracy of the Lipchitz exponent estimation. This may be overcome by using a continuous wavelet transform to obtain a dense sequence of scales, allowing the user to calculate to a higher level of accuracy. This, however, may require significant additional computational time to analyse each signal. Therefore, when using this algorithm for experimental signals it is necessary to use a range of Lipschitz exponents in order to ensure that the singularity corresponding to the shear wave first arrival is determined. For low to moderate noise levels, at which most experimental bender element tests are preformed, an appropriate range of Lipschitz exponents for singularity detection would appear be 0.7 to 1.1. For noisy or very noisy signals a lower range of exponents should be applied.

Experimental Testing

The soil used for testing the wavelet approach was from the Onsøy marine clay test site, located approx. 100 km southeast of Oslo, just north of the city of Fredrikstad. Several research programmes have been carried out by the Norwegian Geotechnical Institute (NGI) at the Onsøy test site over the last 40 years. This uniform marine clay deposit consists of a weathered crust less than 1m thick underlain by 8m of soft clay with iron spots, organic matter and shell fragments and by 36m of homogenous soft to firm plastic clay over bedrock

(Lunne et al. 2003). Each of the tests presented in this paper were performed on Sherbrooke block samples from approximately 10m depth.

An example of the application of the wavelet approach to a bender element signal from an unconsolidated specimen of Onsøy clay (91 mm bender element tip to tip travel distance) with an input frequency of 3 kHz is illustrated in Figure 7. Following the synthetic data testing, Lipschitz exponents in the range of 0.7 to 1.1 were used on the experimental data. This reveals several interesting singularities observed at travel times of 1015 μs, 1430 μs and 1500 μs. The other singularities detected are unlikely to be related to the first arrival of the shear wave and are most likely to have been created by either signal noise or the arrival of reflected waves. Considering the singularities of interest:

- the singularity at 1015 μs is most likely a result of noise, as it would appear to be far too early to be considered as the shear wave arrival. Although this singularity appears to be near what would be expected to be the beginning of the near field, as discussed above, the Lipschitz exponent of the theoretical near-field component will take a value of closer to 2, not 0.91 as measured for this singularity;
- the singular point at 1430 μs is considered to be the point of first arrival of the direct shear wave and produces a shear wave velocity, V_s of 63.6 m/s. As discussed in the next section, in order to improve confidence in the selected singularity, a range of input frequencies should be used, and the corresponding output signals examined for consistent singularities.
- the singular point at 1500 μs could be the arrival of the reflection of the direct shear wave off the bottom cap. This wave will have travelled 95 mm, suggesting a shear wave velocity V_s of 63.3 m/s, similar to that measured for the shear wave first arrival.

Influence of Input Frequency on Different Methods of Travel Time Assessment

As discussed in the introductory section, shear wave arrival times have been estimated by various authors using a number of methods, both in the time and frequency domain. The interpreted travel time from a number of these methods are compared with the wavelet derived time on the same sample of unconsolidated Onsøy clay, as shown in Fig. 8, for a range of frequencies (1 kHz, 3 kHz, 7.5 kHz). All singularities detected between 900 μs and 1750 μs are shown. As illustrated in Figure 8a, for an input frequency of 1 kHz, the received signal is significantly affected by near field effects. As shown, the visual methods produce relatively different travel times (1825 μs and 1730 μs for peak-to-peak and zero-crossing respectively). Similarly the peak cross-correlation function is obtained at 1910 μs. The result produced using the wavelet approach (1430 μs) is considerably different to that observed using the other methods. Each of the other approaches, however, may be strongly dependant on input frequency. As shown on Figure 8b and 8c, and again in Figure 9, (for a greater number of input frequencies) at higher frequencies the estimated travel times from the zero-crossing and peak-to-peak approaches decrease when input frequency increases, eventually converging with the results of the wavelet approach. The cross-correlation approach, which has also been shown to be affected by near field affects at low frequency (Mohsin & Airey 2003) produces a relatively stable result around 1535 μs; this travel time is however significantly higher than that calculated using the other approaches. As shown, the travel time measured by the wavelet approach is not significantly affected by input frequency and varies between 1370 and 1430 μs with an accuracy of ± 32.5 μs.

Using the wavelet approach the first arrival time is well detected from a consistent singularity in the output signals and is independent of input frequency. However, a good quality input signal and a high sampling frequency are necessary to obtain reliable results. In practice it is has been found that the ratio of sampling frequency (f_r) to input frequency (f_i) is

significant. If the ratio of f_r/f_i is maintained above 50, detection of singularities is usually possible and accurate. In general, the travel time is obtained with an accuracy of roughly ± 5 % using the wavelet approach, producing a shear modulus value (G_{max}) with an accuracy of roughly ± 10%, regardless of the presence of strong near-field effects. As discussed above, the DWT limits the accuracy of the Lipschitz exponent estimation. This may be overcome by using a continuous wavelet transform to obtain a dense sequence of scales, allowing the user to calculate to a higher level of accuracy. This however may require significant additional computational time to analyse each signal.

CONCLUSIONS

This paper has introduced and tested a wavelet based approach for the determination of shear wave arrival times from bender element signals. To detect function discontinuity or singularity, a wavelet transform was employed to all signals and local Lipschitz exponents were employed. The local maxima lines of the wavelet transform modulus are observed at different scales, allowing identification of the location of all singularities. By selecting Lipschitz exponents compatible with the input signal it is possible to characterise these singularities, ultimately leading to detection of the singularity relating to the first arrival.

The wavelet approach was tested on both experimental and synthetically generated signals. For the synthetic signals, a consistent singularity, at different levels of noise was observed at the time corresponding to the true arrival. As the Lipschitz exponent corresponding to the true shear wave first arrival decreases with increasing noise level it is recommended that a range of Lipschitz values be used when testing experimental signals. When tested on experimental signals obtained from bender element tests on Onsøy clay, the wavelet approach yielded positive results. Unlike visual assessment approaches, such as the

zero-crossing and peak-to-peak methods, or the cross correlation approach, the wavelet approach is not affected by near field effects and instead was characterised by a relatively consistent singularity across a range of frequencies. One limitation of the wavelet approach appears to be that it is unsuitable for automation and requires the user to select the appropriate singularity relating to the arrival of the shear wave.

ACKNOWLEDGEMENTS

The authors would like to thank Pierse Construction for their funding of the second author. Collection of samples from Onsøy was funded in part by the Norwegian Geotechnical Institute (NGI) and the University of Massachusetts Amherst.

REFERENCES

Arroyo, M., Muir Wood, D. and Greening, P.D. (2003). Source near field effects and pulse tests in soil samples. *Géotechnique* **53**, No. 3, 337-345.

Arroyo, M (2007). Wavelet analysis of pulse tests in soil samples, *Italian Geotechnical Journal*. **30**, No. 2, 26-38.

Arulnathan, R., Boulanger, R.W. and Riemer, M.F. (1998). Analysis of bender element tests, *Geotechnical Testing Journal* **21**, No. 2, 120-131.

Blewett, J., Blewett, I. J., and Woodward, P. K. (1999). Measurement of shear-wave velocity using phase-sensitive detection technique. *Can. Geotech. J.* **36**, No. 5, 934–939.

Brandenberg, S. J., Kutter, B.L. and Wilson, D. W. (2008). Fast Stacking and Phase Corrections of Shear Wave Signals in a Noisy Environment. *J. Geotech. Geoenviron. Eng.* **134**, No. 8, 1154–1165.

Brignoli, E.G.M., Gotti, M. and Stokoe, K.H.II. (1996). Measurement of shear waves in laboratory specimens by means of piezoelectric transducers. *Geotechnical Testing Journal* **19**, No. 4, 384–397.

Brocanelli, D., and Rinaldi, V. (1998). Measurement of low-strain material damping and wave velocity with bender elements in the frequency domain. *Can. Geotech. J.* **35**, No. 6, 1032–1040.

Daubechies, I. (1992). Ten Lectures on Wavelets, *Society for Industrial and Applied Mathematics*, 357 pages.

Donohue, S. (2005). Assessment of sample disturbance in soft clay using shear wave velocity and suction measurements, *PhD Thesis*, University College Dublin.

Donohue, S. and Long, M. (2010). Assessment of sample quality in soft clay using shear wave velocity and suction measurements. Accepted for publication in *Géotechnique*.

Dyvik, R. and Madshus, C., (1985). Lab measurements of G_{max} using bender elements. *Proceedings of the ASCE Conf. On Advances in the Art of Testing Soils under Cyclic Conditions*, Detroit, 186-196.

Dyvik, R. and Olsen, T.S., (1989). G_{max} measured in oedomoter and DSS tests using bender elements. *Proceedings 12th International Conference on Soil Mechanics and Foundation Engineering*, Rio de Janeiro **1**, 39-42.

Greening, P.D., Nash, D.F.T., Benahmed, N., Ferriera, C., and da Fonseca, V (2003). Comparison of shear wave velocity measurements in different materials using time and frequency domain techniques, *Proceedings of the International symposium*, IS-Lyon 03, Lyon. September, 381-386.

Greening, P.D. and Nash, D.F.T. (2004). Frequency domain determination of G_0 using bender elements, *Geotechnical Testing Journal* **27**, No. 3, 288-294

Grossmann, A. and J. Morlet, J. (1984). Decomposition of hardy functions into square integrable wavelets of constant shape. *SIAM Journal of Mathematical Analysis* **15**, No. 4, 723-736

Jardine, R.J., Potts, D.M., Fourie, A.B. and Burland, J.B. (1986). Studies of the Influence of Non-linear Stress-Strain Characteristics in Soil Structure Interaction. *Géotechnique* **36**, No. 3, 377-396.

Jovicic, V., Coop, M.R. and Simic. M. (1996). Objective criteria for determining G_{max} from bender element tests. *Géotechnique* **46**, No. 2, 357-362.

Jovicic, V. and Coop, M.R. (1997). Stiffness of coarse-grained soils at small strains. *Géotechnique* **47**, No. 3, 545-561.

Kawaguchi, T., Mitachi, T and Shibuya, S. (2001). Evaluation of shear wave travel time in laboratory bender element test, *Proceedings of the 15th Int. Conf. Soil. Mech. Found. Eng,* Istanbul **1**, 155-158.

Lee, J.S. and Santamarina, J.C. (2005). Bender Elements: Performance and Signal Interpretation. *J. Geotech. Geoenviron. Eng.* **131**, No. 9, 1063-1070.

Lings, M.L. and Greening, P.D. (2001). A novel bender/extender element for soil testing. *Géotechnique* **51**, No. 8, 713-717.

Lunne, T., Long, M. and Forsberg, C.F. (2003). Characterisation and engineering properties of Onsøy clay. *Characterisation and Engineering Properties of Natural* Soils, Tan et al. (eds) **1**, 395-428, Balkema.

Mallat, S. (1999). *A Wavelet Tour of Signal Processing*, Academic Press.

Mallat, S. and Hwang (1992). Singularity detection and processing with wavelets. *IEEE Transactions on Information Theory* **38**, No. 2, 617-643.

Mohsin, A.K.M. and Airey, D.W. (2003). Automating G_{max} measurement in triaxial tests, *Proceedings of the International symposium, IS-Lyon 03*, Lyon. September.

Mohsin, A.K.M., Donohue, S. and Airey, D.W. (2004). Development of a Simple, Economical, and Robust Method of Estimating G_{max} using Bender Elements, *Proceedings of the 9th Australia New Zealand Conference on Geomechanics*, Auckland **2**, 696-702.

Sanchez-Salinero, I., Roesset, J.M. and Stokoe, K.H. II, (1986). Analytical studies of body wave propagation and attenuation, Report GR 86-15, University of Texas at Austin.

Santamarina, J.C., Klein, K. A. and Fam, M.A. (2001). *Soils and Waves*, J. Wiley and Sons, Chichester, UK, 488 pages.

Shirley, D.J. and Hampton, L.D. (1978) Shear wave measurements in laboratory sediments. *Journal of Acoustical Society of America* **63**, No. 2, 607-613.

Stokoe, K.H., II, Joh, S.H., and Woods, R.D. (2004). Some Contributions of In-situ Geophysical Measurements to Solving Geotechnical Engineering Problems. *Proceedings of the Int. Conf. on Site Characterization 2, ISC 2*, **1**, 97-132, Porto.

Viggiani, G. and Atkinson, J.H. (1995a). Stiffness of fine-grained soil at very small strains. *Géotechnique* **45**, No. 2, 249-265

Viggiani, G. and Atkinson, J.H. (1995b). Interpretation of bender element tests. *Géotechnique* **45**, No. 1, 149-154

Wang, Y. H., Lo, K. F., Yan, W. M., and Dong, X. B. (2007). Measurement biases in the bender element test. *J. Geotech. Geoenviron. Eng.* **133**, No. 5, 564–574.

Zeng, X. and Ni, B. (1998). Application of Bender Elements in measuring G_{max} of sand under K_0 Condition. *ASTM Geotechnical Testing Journal* **21**, No. 3, 251-263

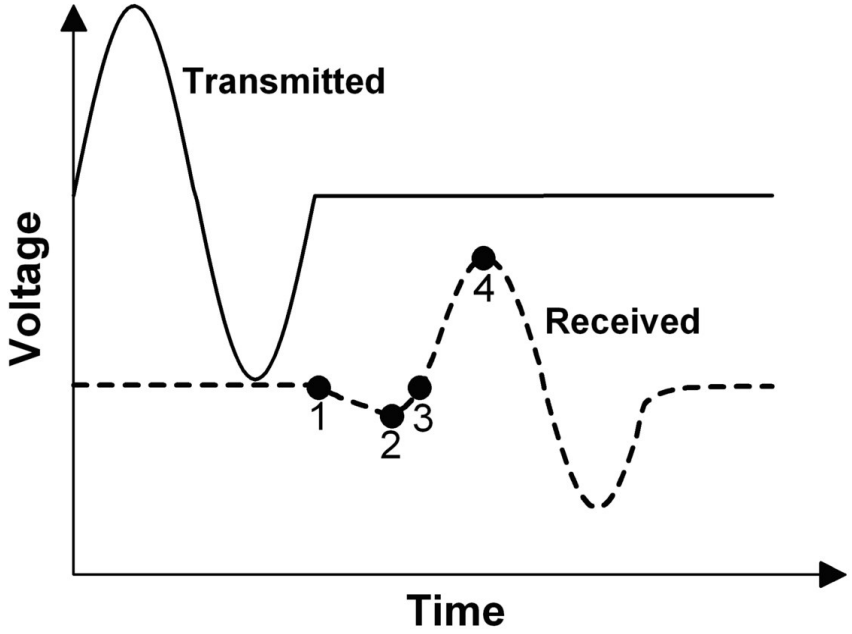

Figure 1. Typical bender element signal received from a transmitted sine pulse. Received signal is within the near field and exhibits characteristic points, 1 at the first deflection, 2 first maximum, 3 zero after first maximum, and 4 first major peak.

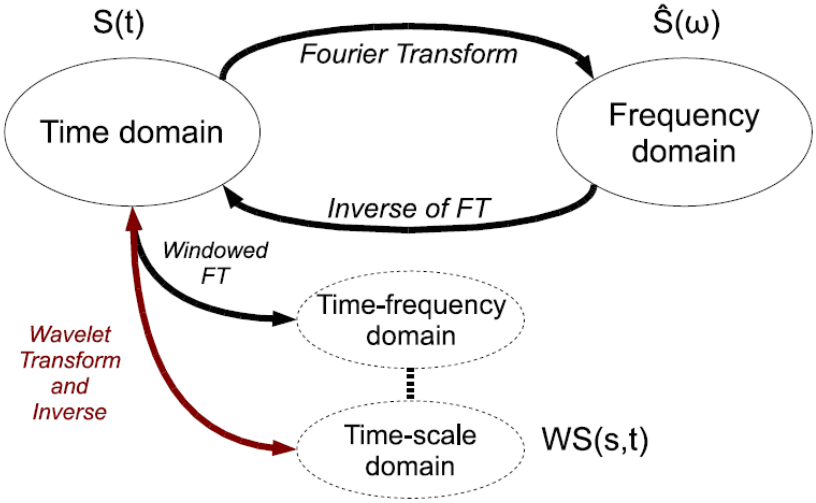

Figure 2. Connection between time and frequency domains.

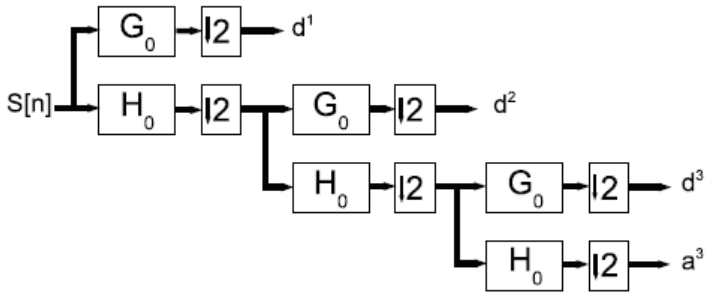

Figure 3. Mallat tree with dyadic sequence of scale (2^j)

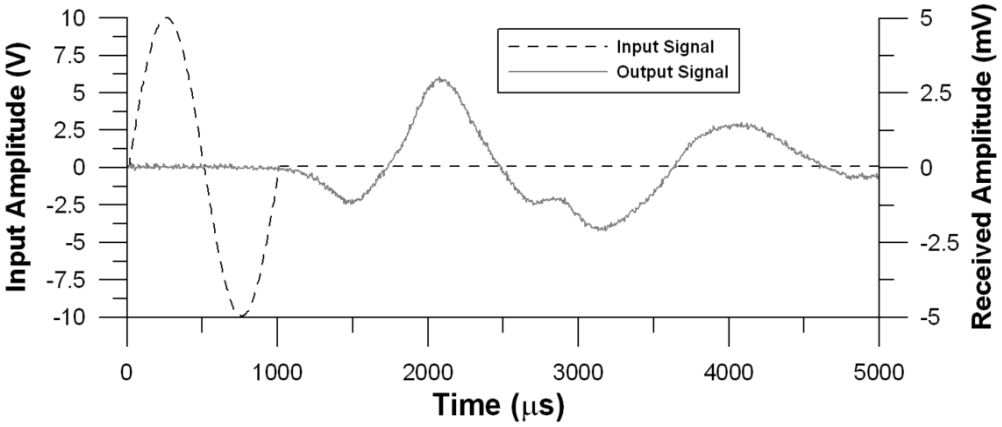

Figure 4. Sample bender element input and output signal, S.

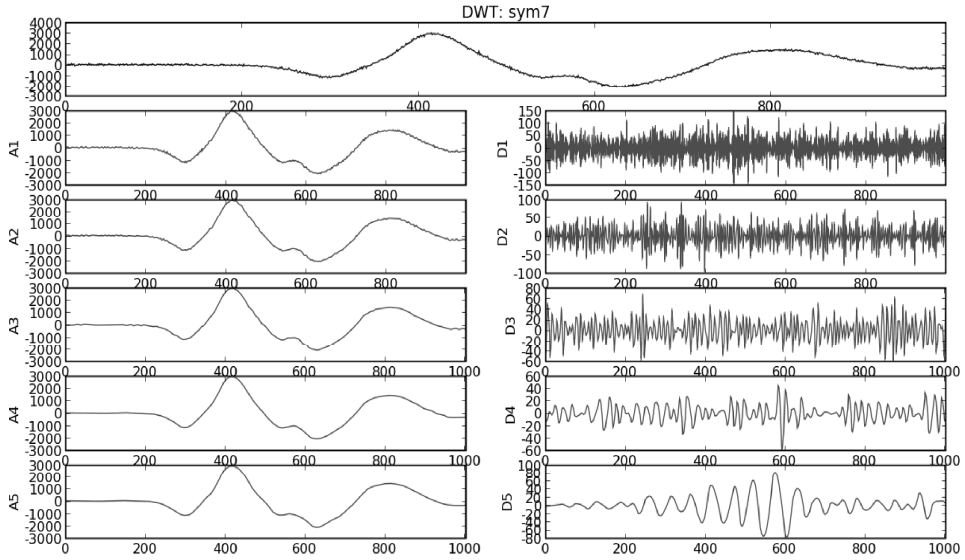

Figure 5. Signal decomposition across a number of scales of S with a Symlet 7.

	Wavelet Type			
	Haar	Daubechies L	Symlet L	Coif L
Explicit expression	Yes	No	No	No
Support width	1	2L - 1	2L - 1	6L - 1
Regularity	Not Regular	≈ 0.3L	≈ 0.3L	≈ 0.6L
Vanishing moments	1	L	L	2L
Symmetrical	No	No	Near	Yes

Table 1: Properties of commonly used support wavelets

	Frequency		
Noise	1 kHz	2.5 kHz	7.5 kHz
None	1.16	1.16	1.52
1%	0.91	1.16	0.92
2%	0.71	1.07	0.93
3%	0.62	0.84	0.70

Table 2: Lipschitz exponents of singularities corresponding to the true shear wave first arrival at different frequencies and noise levels.

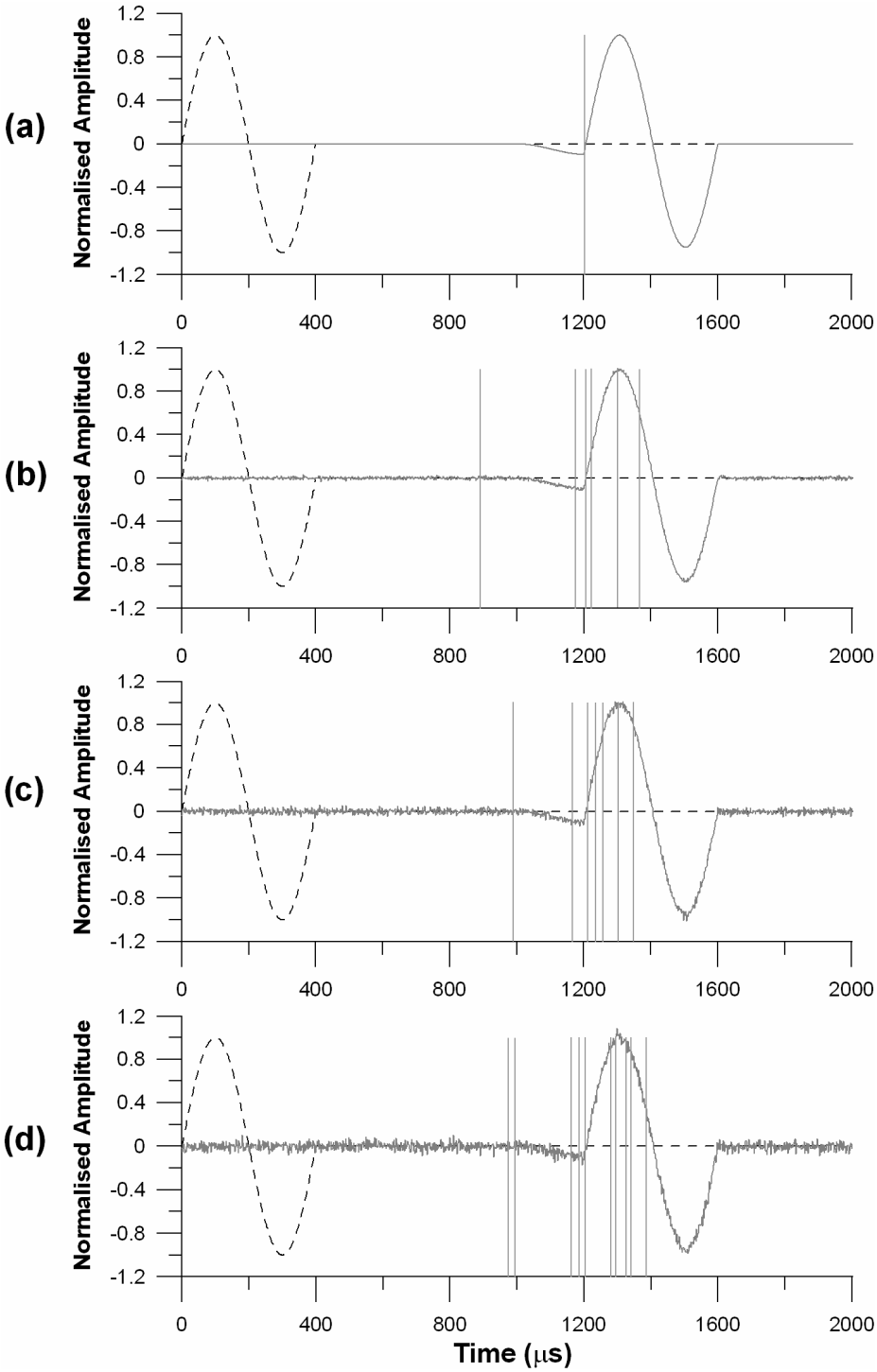

Figure 6. Synthetic signals with an input frequency of 2.5 kHz and corresponding singularities at Gaussian noise levels of (a) zero %, (b) 1%, (c) 2%, and (d) 3%. Shear wave and near field arrival times are 1200 μs and 1100 μs respectively.

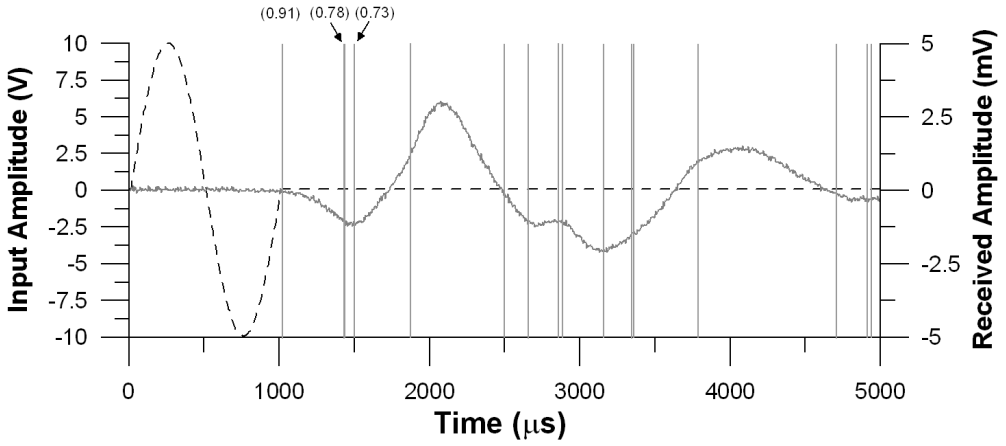

Figure 7. Location of singularities on a sample signal using a symlet 7 and a range from 0.7 to 1.1 of Lipschitz exponents.

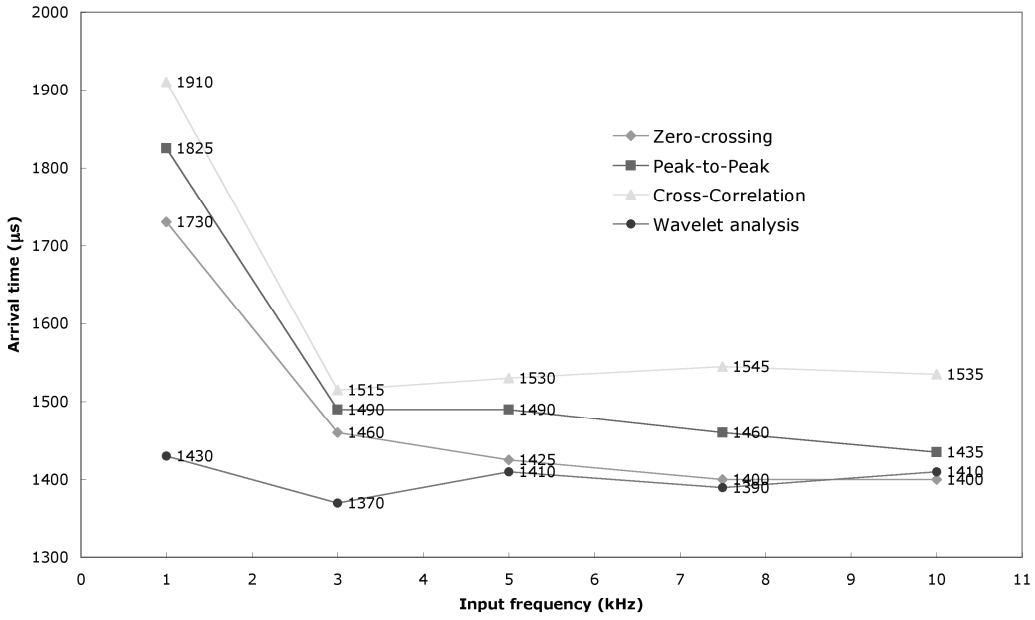

Figure 9. Comparison between travel times measured using four different methods, across a wide range of frequencies (1 – 10 kHz).

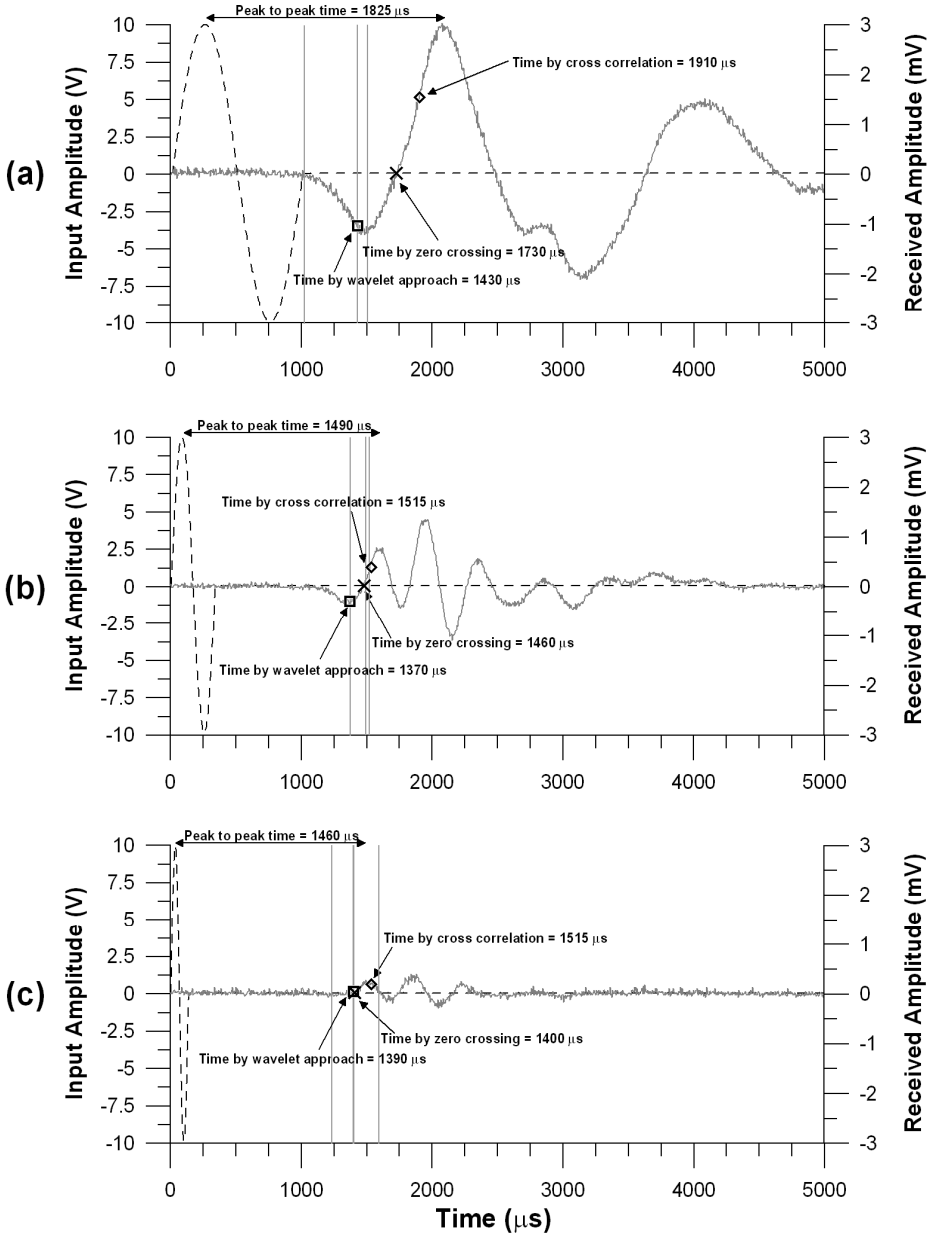

Figure 8. Shear wave arrival times measured using the wavelet, peak-to-peak, zero-crossing and cross correlation methods overlain on received bender element signals for input frequencies of (a) 1kHz, (b) 3kHz and (c) 7.5 kHz.